Mismatch between morphological and functional assessment of the length of coronary artery disease

Mismatch between morphological and functional assessment of the length of coronary artery disease

Maurizio Lodi Rizzini MSc[1]; Sakura Nagumo MD, PhD[2,3], Diego Gallo PhD[1], Jeroen Sonck MD[2,4]; Takuya Mizukami MD, PhD[2,5]; Fabrizio D'Ascenzo MD, PhD[6]; Dimitri Buytaert MSc[2]; Umberto Morbiducci PhD [1]; Bernard De Bruyne MD, PhD[2,7], Claudio Chiastra, PhD[1] and Carlos Collet MD, PhD[2]

1. PoliTo[BIO]Med Lab, Department of Mechanical and Aerospace Engineering, Politecnico di Torino, Turin, Italy
2. Cardiovascular Center Aalst, Onze-Lieve-Vrouw Clinic, Aalst, Belgium
3. Department of Cardiology, Showa University Fujigaoka Hospital, Kanagawa, Japan.
4. Department of Advanced Biomedical Sciences University Federico II, Naples, Italy.
5. Clinical Research Institute for Clinical Pharmacology and Therapeutics, Showa University, Tokyo, Japan
6. Città della Salute e della Scienza Hospital, University of Turin, Turin, Italy
7. Department of Cardiology, Lausanne University Center Hospital, Lausanne, Switzerland

Short title: Functional-anatomical CAD mismatch.

Disclosures: The authors take responsibility for all aspects of the reliability and freedom from bias of the data presented and their discussed interpretation. JS report research grants provided by Cardiopath PhD program. BDB reports receiving research grants from Boston Scientific and Abbott Vascular. ClC, DG and UM were supported by MIUR FISR – FISR2019_03221 CECOMES. CaC reports receiving research grants from Biosensor, Coroventis Research, Medis Medical Imaging, Pie Medical Imaging, Cathworks, Boston Scientific, Siemens, Heart Flow Inc. and Abbott Vascular; and consultancy fees from Heart Flow Inc, Opsens, Abbott Vascular and Philips Volcano.

Address for Correspondence:
Carlos Collet MD, PhD
Cardiovascular Center Aalst, OLV Hospital,
Moorselbaan 164, Aalst, Belgium 9300
Telephone +3253724433
Fax: +32470795867
E-mail: carloscollet@gmail.com
Twitter @ColletCarlos

Structured Abstract

Background: Morphological evaluation of coronary lesion length is a paramount step during invasive assessment of coronary artery disease. Likewise, the extent of epicardial pressure losses can be measured using longitudinal vessel interrogation with fractional flow reserve (FFR) pullbacks. We aimed to quantify the mismatch in lesion length between morphological (based on quantitative coronary angiography, QCA, and optical coherence tomography, OCT) and functional evaluations.

Methods: This is a prospective and multicenter study of patients evaluated by QCA, OCT and motorized fractional flow reserve pullbacks (mFFR). The difference in lesion length between the morphological and functional evaluations was referred to as morphological-functional mismatch.

Results: 117 patients (131 vessels) were included. Median lesion length derived from angiography was 16.05mm [11.40-22.05], from OCT was 28.00mm [16.63-38.00] and from mFFR 67.12mm [25.38-91.37]. There was no correlation between QCA and mFFR lesion length (r=0.124, 95% CI -0.168-0.396, p=0.390). OCT lesions length did correlate with mFFR (r=0.469, 95% CI 0.156-0.696, p=0.004). Morphological-functional mismatch was strongly associated with the improvement in vessel conductance with percutaneous coronary intervention (PCI), higher mismatch was associated with lower post-PCI FFR.

Conclusions: Lesion length assessment differs between morphological and functional evaluations. The morphological-functional mismatch in lesion length is frequent, and influenced the results of PCI in terms of post PCI FFR. Integration of the extent of pressure losses provides clinically relevant information that may be useful for clinical decision-making concerning revascularization strategy.

Key words

Coronary artery disease

Coronary physiology

Fractional flow reserve

Optical coherence tomography

Diffuse disease

Quantitative coronary angiography

Introduction

Invasive functional assessment of coronary artery disease (CAD) has been regarded as the standard of reference for decision making about revascularization in patients with chronic coronary syndromes. Guidelines advocate evaluating the reduction in coronary flow using pressure-derived indices to decide upon the need for revascularization. [1] Intracoronary pressure measurements are typically performed in the distal segment of the coronary artery reflecting cumulative pressure losses along the epicardial vessel. [2] Focal narrowing can be entirely responsible for the pressure drops; nonetheless, diffuse functional deterioration can be also observed outside angiographic stenotic regions contributing to the total decrease in coronary perfusion pressure. [3]

Coronary angiography remains to date the most utilized method to guide stent implantation. The length of the lesion can be quantified by quantitative coronary angiography (QCA), or alternatively, and more precisely, using intravascular imaging. Both approaches aim to guide stent length selection to restore epicardial conductance and improve myocardial perfusion. In almost a third of patients, however, after an angiographically successful PCI, epicardial conductance remains suboptimal. [4] Patients with persistent low FFR after percutaneous revascularization appear to be at an increased risk of adverse events. [4]

A pullback maneuver during intracoronary pressure measurements identifies the presence, location, magnitude and extent of pressure drops. [5] Two factors, namely (i) the magnitude of FFR drops and (ii) extension of functional CAD, are predictive of improvement in epicardial conductance after percutaneous revascularization. [3] Thus, quantifying the extent of functional CAD may have prognostic capability for post-PCI FFR.

Our aim was to quantify the mismatch in the extent of CAD between morphological and functional evaluations and to assess the impact of the morphological and functional mismatch on FFR after PCI.

Methods

Study design

This is a multicenter, prospective registry of patients undergoing clinically indicated coronary angiography in whom motorized FFR pullback evaluations were performed before PCI. Patients presenting with acute coronary syndromes, previous coronary artery bypass grafting, significant valvular disease, severe obstructive pulmonary disease or bronchial asthma, coronary ostial lesions, severe tortuosity, or severe calcification were excluded. Patients with adequate pressure tracings and pullback curves were included in this analysis. The study was approved by the Ethics Committee at each participating center. The study population is a combination of two prospective studies NCT03824600 and NCT03782688.

Coronary angiographic analysis

Angiographies were performed using a dedicated acquisition protocol. Two angiographic projections separated at least 30 degrees were obtained for each target lesion after the administration of intracoronary nitrates (**Figure 1A**). Angiograms were evaluated blinded to physiological and clinical data and were analyzed using three-dimensional quantitative coronary angiography (QCA) (QAngio XA, Medis Medical Imaging, Netherlands). Minimal lumen diameter (MLD), reference vessel diameter (RVD), and percentage diameter stenosis (%DS) were calculated. Acute gain was defined as the difference between post and pre-PCI MLD. Manual correction of anatomical lesion length was not allowed. Serial lesions were defined as the presence of at least two >50% visual diameter stenosis lesions within the same vessel, at a distance of at least three times the reference vessel diameter.[6] QCA-derived anatomical lesion length expressed in millimeters was calculated using the 3D QCA software and defined as the length where the reference diameter line intersects the diameter function line (**Figure 1B**).

Optical Coherence Tomography

Examinations were performed using the OPTIS™ OCT systems (Abbott Vascular). OCT pullbacks at 36mm/s were acquired before pre-dilation if feasible. Stent diameter selection was based on the distal reference mean external elastic lamina (EEL)-based diameters rounded down to the nearest available stent size (usually in 0.25 mm increments) to determine stent diameter. If the EEL could not be adequately visualized, the stent diameter is chosen using the mean lumen diameter at the distal reference

rounded up to the next stent size. Optimization of the device was performed based on OCT at operator discretion. OCT-derived anatomical lesion length expressed in millimeters was defined as the distance between the proximal and distal reference segments using the OCT automated lumen detection feature. [7]

Intracoronary pressure measurement and FFR pullback curve analysis

Fractional flow reserve (FFR) measurements were performed with the PressureWire X (Abbott Vascular, Chicago, Il, USA) that was connected to a motorized pullback device at a speed of 1 mm/s (R 100, Philips Volcano, San Diego, Ca, USA). Pressure pullback measurements were acquired at a sampling frequency of 100 Hz. A continuous intravenous adenosine infusion was given at a dose of 140 μg/kg/min via a peripheral or central vein to obtain steady-state hyperemia for at least 2 min. [2] The position of the pressure sensor was recorded with a contrast injection to identify the pullback initial position for co-registration purposes. In cases undergoing PCI, FFR measurements were repeated at the same anatomical location. FFR gain was defined as FFR post-PCI minus FFR pre-PCI. If FFR drift (>0.03) was observed, the FFR pullback was repeated.

The FFR curve along the vessel axis was reconstructed by applying a moving average filter with a window size of 10 s, followed by an infinite impulse response low pass elliptic filter (0.1 Hz cutoff frequency) for smoothing (**Figure 1C**). An automatic algorithm was developed for functional length quantification from FFR curves. The first step of the algorithm consisted in the piece-wise linearization of each FFR curve (**Figure 1C**) by applying an automated change-points detection algorithm based on a penalized parametric global method, as detailed in the Supplementary Materials (Supplementary Methods, section "Change points detection on FFR pullback curves"). The second step of the algorithm consisted in the automatic classification of the linearized FFR curve segments as 'healthy' segments (i.e. without FFR deterioration), 'focal' or 'diffuse' disease segments (**Figure 1C**), based on their length and the associated FFR drop.

Two cohorts were defined to develop and validate the part of the algorithm performing automatic FFR segments classification. The derivation cohort consisted of patients with CAD defined as distal FFR<0.90. For this cohort, only baseline (i.e. pre-PCI) FFR pullbacks were included. These were

selected in a consecutive fashion from all patients included in the registry. The validation cohort included subsequent patients with CAD defined as a distal FFR ≤0.80 who underwent OCT-guided PCI and FFR measurement after stent implantation.

Two independent observers (observer 1: CaC; observer 2: SN) preliminarily adjudicated by visual inspection each one of the piece-wise linearized FFR curve segments belonging to the two cohorts as 'healthy', i.e. without FFR deterioration, or as 'diseased'. Then, the two observers performed a further adjudication on 'diseased' segments, discriminating between 'focal' or 'diffuse', based on the presence of step-ups in the FFR pullback linearized curve.

The visual adjudication of the derivation cohort was used to develop the automatic classifier, based on a two-variables logistic regression. The two independent variables considered for the logistic regression were the length of the linearized segment and the associated FFR drop. Further details about the automatic classifier are reported in the Supplementary Materials (Supplementary Methods, section "Automatic segments classification").

Functional length of CAD, expressed in millimeters, was defined as the length of the pressure pull-back curve with FFR deterioration. To calculate functional length, an automatic piece-wise linearization and classification of the FFR curve segments was developed. In detail, the functional length of disease for each coronary artery was obtained as the summation of the length of all linearized FFR curve segments classified as diseased by the algorithm. In the presence of serial or multiple lesions (i.e. functionally diseased segments separated by functionally healthy segments), the functional length was considered as the sum of all (i.e., contiguous and non-contiguous) diseased segments.

Functional-anatomical mismatch (FAM)

The difference between the anatomical and the functional length of CAD was defined as Functional Anatomical Mismatch (FAM) (**Figure 1D**). This quantity allows identifying two lesion endotypes: (1) functional disease circumscribed within the anatomical defined lesion (i.e. FAM>0), and (2) functional disease extending beyond the anatomical defined lesion (FAM<0). A positive FAM represents focal CAD where the functional length of disease is restricted to the lesion length, whereas a negative FAM

value points to the presence of functional disease outside the anatomical lesion (**Figure 2**). For visualization purposes, FAM values were colored-coded using the 3D QCA geometries inside the anatomical lesion with positive values shown in red and negative values in blue (**Figure 2**). As the anatomical length of CAD can be derived from QCA or OCT, two FAM values were calculated, namely FAM_{QCA} and FAM_{OCT} (**Figure 3)**. In addition, the proportion of pressure loss contained within the anatomical lesion defined the FFR drop attributable to the QCA or OCT-derived anatomical lesion relative to the FFR drop of the entire vessel (i.e. FFR drop within QCA or OCT lesion, respectively).

Procedure guidance and results

PCI was performed following standard of care guided by FFR and OCT, both executed before and after stent implantation. Intraprocedural PCI guidance or stent optimizations based on either physiology or imaging were left at operator's discretion. New generation DES were used in all cases. To quantify the impact of PCI, the relative functional gain was defined as post PCI FFR minus pre-PCI FFR divided by 1 – pre-PCI FFR.

Statistical analysis

Continuous data are presented as mean (±SD) or median [25th – 75th percentiles]. Categorical data are presented as counts and proportions (%). Differences were evaluated using the univariate Mann–Whitney non-parametric U test. Spearman's correlation coefficients were calculated to assess the relationship between FAM and post-PCI FFR. Agreement between observers was assessed by the intraclass correlation coefficient (ICC). The optimal cutoff values of FAM to predict relative functional gain were calculated using receiver operating characteristic (ROC) curves. The discriminant ability of FAM value to predict optimal post-PCI physiologic results was evaluated with area under curve (AUC). Optimal relative functional gain was defined as an increase in epicardial conductance greater than 50%.

Results

Clinical characteristics of patients are shown in **Table 1**. Overall, 117 patients (131 vessels) were included: 71 patients (81 vessels) in the derivation cohort and 48 patients (50 vessels) in the validation cohorts. In the validation cohort, QCA and OCT lesion lengths were available for 50 and 36 vessels,

respectively (**Table 2**). FFR motorized pullbacks pre and post PCI were available in all cases. The relationship between FFR and QCA-based MLA and QCA-based MLD are shown in Supplementary Materials. The existence of possible links between OCT-based and QCA-based evaluations was also probed. The results are presented in the Supplementary Materials.

FFR pullback curve automatic classifier

Anatomical, functional, and procedural characteristics of the derivation and validation cohort are presented in **Table 2**. From the FFR curves, 431 segments were extracted. In detail, 151 (observer 1) and 156 (observer 2) segments were visually assessed as healthy, 101 (observer 1) and 106 (observer 2) as focal disease,146 (observer 1) and 147 (observer 2) as diffuse disease (**Figure 4**). In the validation cohort, the automatic classifier provided an excellent discrimination ability between 'healthy' and 'diseased' segments (AUC was 0.97, 95% CI 0.94 to 0.99 for observer 1, and 1.00, 95% CI 0.98 to 1.00 for observer 2). Concerning differentiation between focal and diffuse, the discriminatory capacity was also excellent (AUC was 0.93, 95% CI 0.86 to 0.97 for observer 1, and 0.96, 95% CI 0.91 to 0.99 for observer 2). The inter-observer agreement for the visual evaluation of the FFR curve was moderate (ICC 0.66, 95% CI 0.60 to 0.71), whereas the reproducibility for the automatic algorithm was excellent because the algorithm is based on a deterministic approach.

Functional Anatomical Mismatch

PCI was performed in 50 vessels included in the validation cohort. Pre-PCI FFR was 0.74 [0.67 – 0.77] and diameters stenosis was 53.0 % [47.25 – 59.50]. Anatomical CAD length derived from QCA was 16.05 mm [11.40 – 22.05], anatomical CAD length derived from OCT was 28.0 mm [16.63 – 38.0] and functional CAD length was 67.12 mm [25.38 – 91.37] ($p<0.001$). No correlation emerged between the extent of CAD derived from QCA and FFR pullback (r=0.124, 95% CI 0.168 to 0.396, p=0.390, **Figure 5A**). OCT-derived anatomical lesion length was correlated with functional CAD length (r=0.469, 95% CI 0.156 to 0.696, p=0.004, **Figure 5B**).

Mean stent length was 27.45 ± 11.52 mm. Mean post-PCI FFR was 0.86 [0.82 – 0.89]. An explanatory example visualizing vessels with positive and negative FAM that underwent PCI and post-PCI FFR

measurement is presented in **Figure 2**. FAM_{QCA} was -47.59 [-73.22 – -8.08] mm and FAM_{OCT} was -37.47 [-64.29 – -8.98] mm (p=0.446). The length of functional CAD was inversely correlated with relative functional gain (r=-0.672, 95% CI -0.804 to -0.478, p<0.001, **Figure 5C**) i.e., the longer the functional disease, the lesser the improvement in FFR with PCI. A strong association emerged between FAM_{QCA} and FFR relative gain after PCI (r=0.647, 95% CI 0.443 to 0.788, p<0.001, **Figure 6A**), as well as between FAM_{OCT} and FFR relative gain after PCI (r=0.630, 95% CI 0.372 to 0.798, p<0.001, **Figure 6B**). A sensitivity analysis in the sub-group of serial lesions showed similar results as reported in Supplementary Materials**.**

Patients in whom functional disease was confined within the anatomical lesion (i.e. FAM ≥0) had the strongest improvement in relative functional gain (FAM_{QCA}≥ 0.701 ± 0.235 vs. FAM_{QCA} <0 0.441 ± 0.225, p<0.001). FAM either derived from QCA or OCT predicted functional gain (FAM_{QCA} AUC 0.84, 95% CI 0.71 to 0.93, p<0.001 and FAM_{OCT} AUC 1.00, 95% CI 0.93 to 1.00, p<0.001). The best FAM_{QCA} and FAM_{OCT} cut-off values predicting 50% gain in epicardial conductance were -57.64 mm and -37.19 mm, respectively. Percent FFR drops within the anatomical lesions either derived from QCA or OCT were strongly correlated with functional gain (r=0.792, 95% CI 0.655 to 0.879, p<0.001 for QCA and r=0.789, 95% CI 0.615 to 0.890, p<0.001 for OCT, **Figure 6C-6D**).

Discussion

The present study describes a novel approach for the quantification of the extension of functional CAD. This allowed to determine the mismatch in the extent of CAD between anatomical and physiological invasive evaluations based on angiography, intravascular imaging and intracoronary hyperemic pressure tracing pullbacks. The main findings can be summarized as: (1) the extent of functional disease derived from FFR pullback curves can be quantified using an automated algorithm; (2) in patients with hemodynamically significant coronary stenosis, lesion length based on QCA and CAD length based on FFR pullbacks were not correlated. In contrast, CAD length derived from OCT correlated with functional CAD extent; (3) the mismatch between the length of anatomical and functional CAD (i.e. FAM, either derived from QCA or OCT) correlated with the improvement in epicardial conductance after percutaneous revascularization.

The discordance between anatomy and physiology regarding epicardial lesion severity has been widely recognized. In the FAME study, more than one-third of lesions with an angiographic 50% to 70% diameter stenosis demonstrated an FFR ≤0.80 whereas one-fifth of lesions with a 71% to 90% angiographic diameter stenosis demonstrated an FFR > 0.80. [8] Disconnection between anatomy and physiology goes beyond the assessment of lesion significance. The length of CAD also differs between anatomical and functional evaluations. In the present study, length of functional disease was greater than its anatomical equivalent either derived from QCA or OCT (i.e., those with FAM<0, **Figure 6**). QCA is based on conventional angiography and identifies CAD length as the extent of the stenotic segment. On the other hand, OCT, possessing higher spatial resolution, derives lesion length from the selection of proximal and distal reference cross-sections without atherosclerotic plaques. Therefore, it is expected that CAD anatomical length derived from OCT will be equal or longer than the QCA-derived length. We observed that the anatomical length of CAD was shorter when derived from QCA compared to the one derived from OCT; still, FFR pullbacks derived CAD length was longer (**Figure 6**). This finding highlights the diffuse nature of atherosclerosis when assessed using coronary physiology. Interestingly, CAD extent derived from QCA and functional length were not statistically correlated, whereas OCT-derived anatomical length and functional length exhibited a moderate correlation. These results underline the suboptimal guidance offered by QCA in terms of the evaluation of lesion extension and confirms the usefulness of intravascular imaging for attaining functional complete revascularization.

Pressure pullbacks can show two distinct functional CAD endotypes, namely predominant focal or diffuse. [3] In the focal functional CAD, pressure drops are commonly restricted to anatomical stenosis. In this disease endotype, PCI restores epicardial conductance, results in higher post-PCI FFR, increases the likelihood of relieving patients from angina and is associated with improved clinical outcomes. In contrast, in patients with functional diffuse disease, PCI results in minor improvement in vessel physiology, low post-PCI FFR and higher likelihood of persistent angina. [9] In the present study, we developed an approach to predict the response to PCI by quantifying the extent of functional CAD from FFR pullbacks. The larger the functional length of CAD, the lower the functional gain obtained with

PCI and the lower the likelihood of functional revascularization. With the current approach, the length of functional disease is computed based on an automated algorithm classifying the FFR curve segments as healthy or diseased. This approach may be less vulnerable to artefacts in the pullback curves compared to the application of a threshold. Moreover, the FAM concept by incorporating the anatomical length of the disease accounts for the interaction with PCI, thus assessing the functional contribution in the context of the segment to be treated.

FAM quantifies the mismatch between the anatomical and functional CAD length thereby stressing the impact of residual pressure losses outside the treated region on post PCI physiology. Moreover, the FAM approach is based on the presence and length of disease rather than on the magnitude of pressure drops, making this approach less influenced by the interaction in cases of serial lesions. Furthermore, the functional contribution of the treated lesion, reported in this study as relative FFR drop within the lesion, also correlated with functional gain (**Figure 6, C** and **D**). The larger the delta lesion FFR, the larger the functional gain. Altogether, these findings further support pressure pullback strategies to guide PCI as a second level of decision making after the confirmation of hemodynamic lesion significance.

By identifying lesions with negative FAM where the functional extent of CAD is longer than the anatomical CAD, a dilemma is posed upon clinicians. Extending the treated region with longer stents covering the functional disease may improve post-PCI FFR but it may also lead to longer and more stents, which has been associated with higher rates of target vessel failure. [10, 11] Moreover, PCI in vessels with functional diffuse disease has been associated with more periprocedural complications. [3] Therefore, the assessment of the functional pattern of CAD provides further risk stratification, may improve patient selection for PCI by avoiding stenting lesions without pullback step ups, reduce the risk of peri-procedural myocardial infarction and results in a net clinical benefit from revascularization. It can be hypothesized that patients with negative FAM, i.e. diffuse functional CAD, may be better treated with optimal medical therapy or coronary artery bypass grafting whereas patients with positive FAM are better treated with PCI. Further studies are required to assess the treatment strategies in patients with chronic coronary syndromes and diffuse CAD.

Limitations

The present study has several limitations. First, the performance of FAM is presented based on its relationship with post PCI FFR and not directly with clinical outcomes. Nonetheless, post-PCI FFR have identified as an independent predictor of adverse events after PCI. Second, the sample size of the study was relatively small; however, this is one of the most completely evaluated cohorts with motorized FFR pullbacks and OCT pre- and post-PCI. Third, we were able to validate the FAM concept internally; an external validation is still warranted.

Conclusion

Lesion length assessment differs between morphological and functional evaluations. The morphological functional mismatch in lesion length was frequent, often large, and influenced the results of PCI in terms of coronary physiology. Integration of the extent of pressure losses provides clinically relevant information that may be useful during PCI.

References

[1] Knuuti J, Wijns W, Saraste A, Capodanno D, Barbato E, Funck-Brentano C, et al. 2019 ESC Guidelines for the diagnosis and management of chronic coronary syndromes: The Task Force for the diagnosis and management of chronic coronary syndromes of the European Society of Cardiology (ESC). European heart journal. 2019.

[2] Toth GG, Johnson NP, Jeremias A, Pellicano M, Vranckx P, Fearon WF, et al. Standardization of Fractional Flow Reserve Measurements. Journal of the American College of Cardiology. 2016;68:742-53.

[3] Collet C, Sonck J, Vandeloo B, Mizukami T, Roosens B, Lochy S, et al. Measurement of Hyperemic Pullback Pressure Gradients to Characterize Patterns of Coronary Atherosclerosis. Journal of the American College of Cardiology. 2019;74:1772-84.

[4] Piroth Z, Toth GG, Tonino PAL, Barbato E, Aghlmandi S, Curzen N, et al. Prognostic Value of Fractional Flow Reserve Measured Immediately After Drug-Eluting Stent Implantation. Circulation Cardiovascular interventions. 2017;10.

[5] J S. Influence of the PPG on the results of percutaneous coronary interventions. EuroPCR 2020.

[6] Sianos G, Morel MA, Kappetein AP, Morice MC, Colombo A, Dawkins K, et al. The SYNTAX Score: an angiographic tool grading the complexity of coronary artery disease. EuroIntervention : journal of EuroPCR in collaboration with the Working Group on Interventional Cardiology of the European Society of Cardiology. 2005;1:219-27.

[7] Ali ZA, Maehara A, Genereux P, Shlofmitz RA, Fabbiocchi F, Nazif TM, et al. Optical coherence tomography compared with intravascular ultrasound and with angiography to guide coronary stent implantation (ILUMIEN III: OPTIMIZE PCI): a randomised controlled trial. Lancet (London, England). 2016;388:2618-28.

[8] Tonino PA, De Bruyne B, Pijls NH, Siebert U, Ikeno F, van' t Veer M, et al. Fractional flow reserve versus angiography for guiding percutaneous coronary intervention. The New England journal of medicine. 2009;360:213-24.

[9] Fournier S, Ciccarelli G, Toth GG, Milkas A, Xaplanteris P, Tonino PAL, et al. Association of Improvement in Fractional Flow Reserve With Outcomes, Including Symptomatic Relief, After Percutaneous Coronary Intervention. JAMA cardiology. 2019;4:370-4.

[10] Maron DJ, Hochman JS, Reynolds HR, Bangalore S, O'Brien SM, Boden WE, et al. Initial Invasive or Conservative Strategy for Stable Coronary Disease. The New England journal of medicine. 2020;382:1395-407.

[11] Hwang D, Lee JM, Yang S, Chang M, Zhang J, Choi KH, et al. Role of Post-Stent Physiological Assessment in a Risk Prediction Model After Coronary Stent Implantation. JACC Cardiovascular interventions. 2020;13:1639-50.

Tables

Table 1. Baseline clinical characteristics

	All	Derivation Cohort	Validation Cohort
Patients, n	117	69*	48
Vessels, n	131	81	50
Age, mean ± SD	66.9 ± 9.84	68.2 ± 9.6	64.7 ± 9.9
Sex, male, n (%)	86 (73.5)	52 (73.2)	36 (75.0)
BMI, kg/m2, mean ± SD	26.8 ± 3.53	26.7 ± 3.52	26.8 ± 3.32
Hyperlipidemia, n (%)	94 (80.3)	57 (80.3)	38 (79.2)
Hypertension, n (%)	63 (53.8)	36 (50.7)	29 (60.4)
Diabetes Mellitus, n (%)	26 (22.2)	17 (23.9)	9 (18.8)
Current smoking, n (%)	20 (17.1)	12 (16.9)	9 (18.8)
Family history, n (%)	17 (14.5)	10 (14.1)	8 (16.7)
Previous stroke, n (%)	3 (2.6)	3 (4.2)	0 (0)
Prior PCI, n (%)	32 (27.4)	28 (39.4)	4 (8.3)
LVEF, %, mean ± SD	58.0 ± 8.06	58.1 ± 9.28	58.0 ± 5.57
Creatinine, mg/dl, mean ± SD	0.98 ± 0.22	0.99 ± 0.24	0.96 ± 0.18
Symptomatic, n (%)	91 (77.8)	50 (70.4)	43 (89.6)
Angina Class, CCS			
1	26 (28.6)	15 (30.0)	11 (25.6)
2	61 (67.0)	32 (64.0)	31 (72.1)
3	4 (4.4)	3 (6.0)	1 (2.3)
4	0 (0)	0 (0)	0 (0)

* In two patients, two vessels were analyzed and one underwent PCI. For patient level characteristic these were included in the validation cohort. PCI Percutaneous coronary interventions, CCS Canadian classification society, LVEF Left ventricular ejection fraction, BMI Body mass index, SD Standard deviation

Table 2. Anatomical, functional and procedural characteristics

	All	Derivation Cohort	Validation Cohort
Target vessel, n (%)			
LAD	99 (75.6)	57 (70.4)	42 (84.0)
LCX	9 (6.9)	6 (7.4)	3 (6.0)
RCA	23 (17.6)	18 (22.2)	5 (10.0)
Serial lesion, n (%)	17 (13.0)	9 (11.1)	8 (16.0)
QCA-derived anatomical lesion length (mm), median [25th – 75th percentile]	NA	NA	16.05 [11.40 – 22.05]
OCT-derived anatomical lesion length (mm), median [25th – 75th percentile]	NA	NA	28.00 [16.63 – 38.00]
MLD (mm), median [25th – 75th percentile]	NA	NA	1.34 [1.23 – 1.48]
DS (%), median [25th – 75th percentile]	NA	NA	53.00 [47.25 – 59.50]
RVD (mm), median [25th – 75th percentile]	NA	NA	2.95 [2.57 – 3.20]
Functional lesion length (mm), median [25th – 75th percentile]	NA	NA	67.12 [25.38 – 91.37]
FAM_{QCA} (mm), median [25th – 75th percentile]	NA	NA	-47.59 [-73.22 – -8.08]
FAM_{OCT} (mm), median [25th – 75th percentile]	NA	NA	-37.47 [-64.29 – -8.98]
Pre PCI FFR, median [25th – 75th percentile]	0.78 [0.71 – 0.86]	0.82 [0.73 – 0.88]	0.74 [0.67 – 0.77]
PCI, number	NA	NA	54
Stent per vessel, n (%)	NA	NA	1.00 [1.00, 1.00]
Stent length (mm)	NA	NA	27.45 ± 11.52 mm
Stent diameter (mm)	NA	NA	3.05± 0.43
Post dilatation, n (%),	NA	NA	46 (85.2)
OCT-guided PCI, n (%)	NA	NA	42 (84.0)
MSA (mm^2), median [25th – 75th percentile]	NA	NA	5.66 [4.33 – 6.45]
Residual DS (%), median [25th – 75th percentile]	NA	NA	7.00 [2.00 – 12.00]
Acute gain	NA	NA	1.34 ± 0.54
Post PCI FFR, median [25th – 75th percentile]	NA	NA	0.86 [0.82 – 0.89]
Relative functional gain, median [25th – 75th percentile]	NA	NA	0.49 [0.30 – 0.62]

LAD left anterior descending artery. LCX left circumflex artery. RCA right coronary artery. FAM functional anatomical mismatch. PCI percutaneous coronary interventions. MLD minimal lumen diameter. QCA quantitative coronary angiography. FFR fractional flow reserve. DS diameter stenosis. OCT optical coherence tomography. RVD reference vessel diameter. NA not available.

Figures

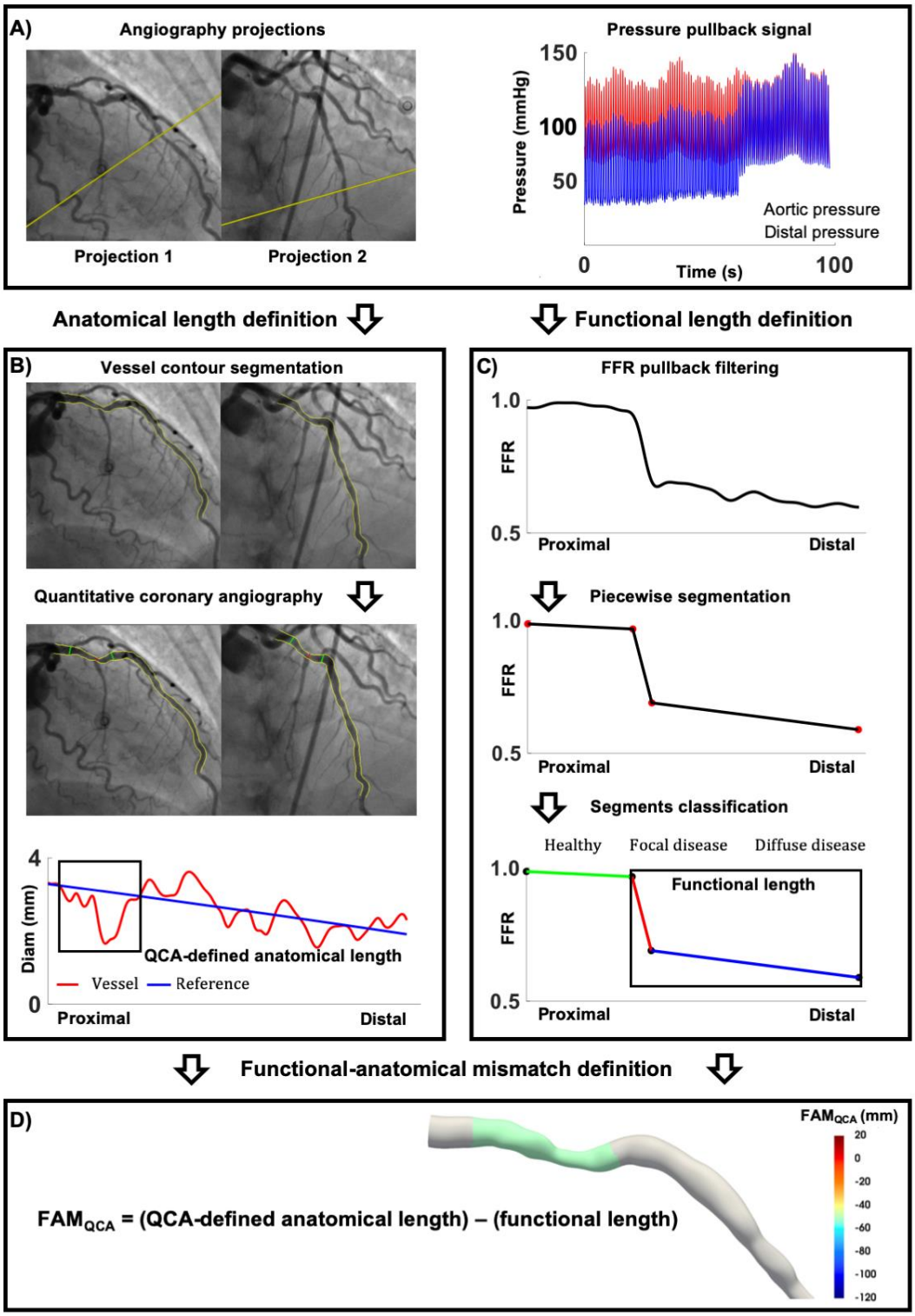

Figure 1. Definition of QCA-derived anatomical lesion length, functional lesion length and functional-anatomical mismatch (FAM_{QCA}). A): The QCA-derived anatomical lesion length was obtained starting from two angiographic projections for each target lesion. B): 3D quantitative coronary angiography

algorithm was used to obtain the QCA-derived anatomical lesion length as the distance where the reference diameter line intersects with the curve describing the local vessel diameter value. C): The functional lesion length was obtained from analysis of the FFR pullback curve after smoothing and piece-wise linearization as the sum of the segments characterized by FFR deterioration. D): The FAM_{QCA} is defined as the difference between the QCA-derived anatomical lesion length minus the functional lesion length.

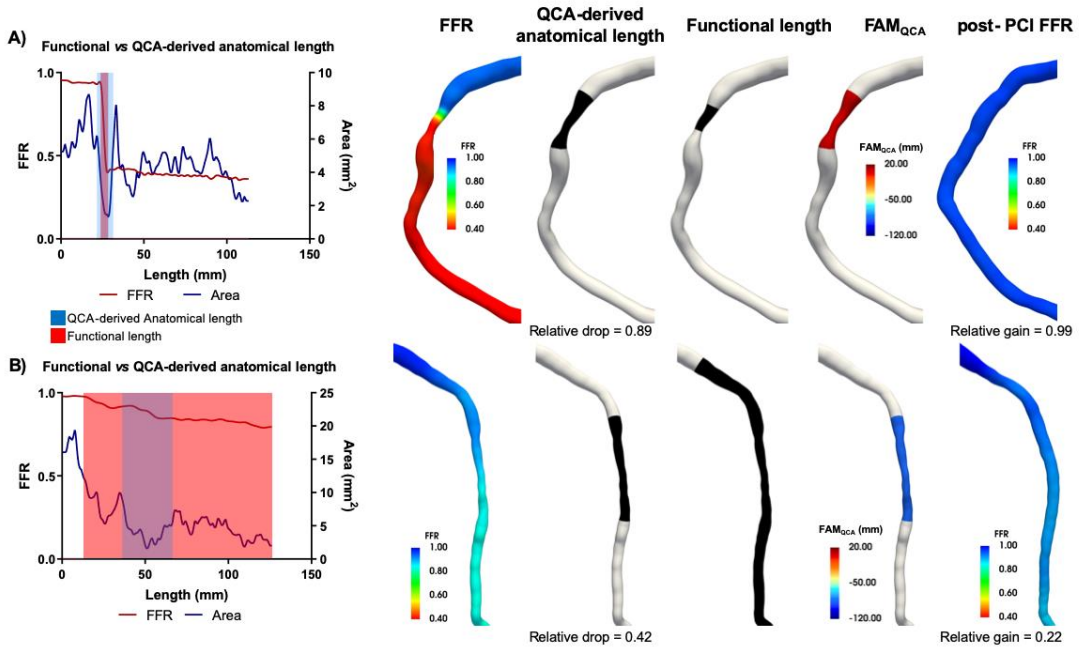

Figure 2. Positive vs. negative FAM_{QCA}. A): example of vessel with positive FAM_{QCA}, where the QCA-derived anatomical lesion length is longer than the functional lesion length, respectively blue and red shade in the area and FFR curves (left panel). From left to right, FFR is displayed as a color-coded map on the 3-dimensional geometric reconstruction of the vessel. The extension of the anatomical and functional length is displayed in black, with indication of the relative FFR drop within the QCA-derived anatomical lesion. FAM_{QCA} is displayed as a color-coded map: the red color underlines that the functional disease was circumscribed within the anatomical lesion. The percutaneous coronary intervention (PCI) restored epicardial conductance and resulted in high post-PCI FFR (right panel), with a relative gain equal to 0.99. B): example of vessel with negative FAM_{QCA}, where the anatomical lesion length is shorter than the functional lesion length, respectively blue and red shade in the area and FFR curves (left panel). From left to right, FFR is displayed as a color-coded map on the 3-dimensional geometric reconstruction of the vessel. The extension of the QCA-derived anatomical and functional length is displayed in black, with indication of the relative FFR drop within the anatomical lesion. FAM_{QCA} is displayed as a color-coded map: the blue color underlines that the functional disease extended beyond the anatomical lesion. The percutaneous coronary intervention (PCI) resulted in minor improvement of epicardial conductance and a low post-PCI FFR (right panel), with a relative gain equal to 0.22.

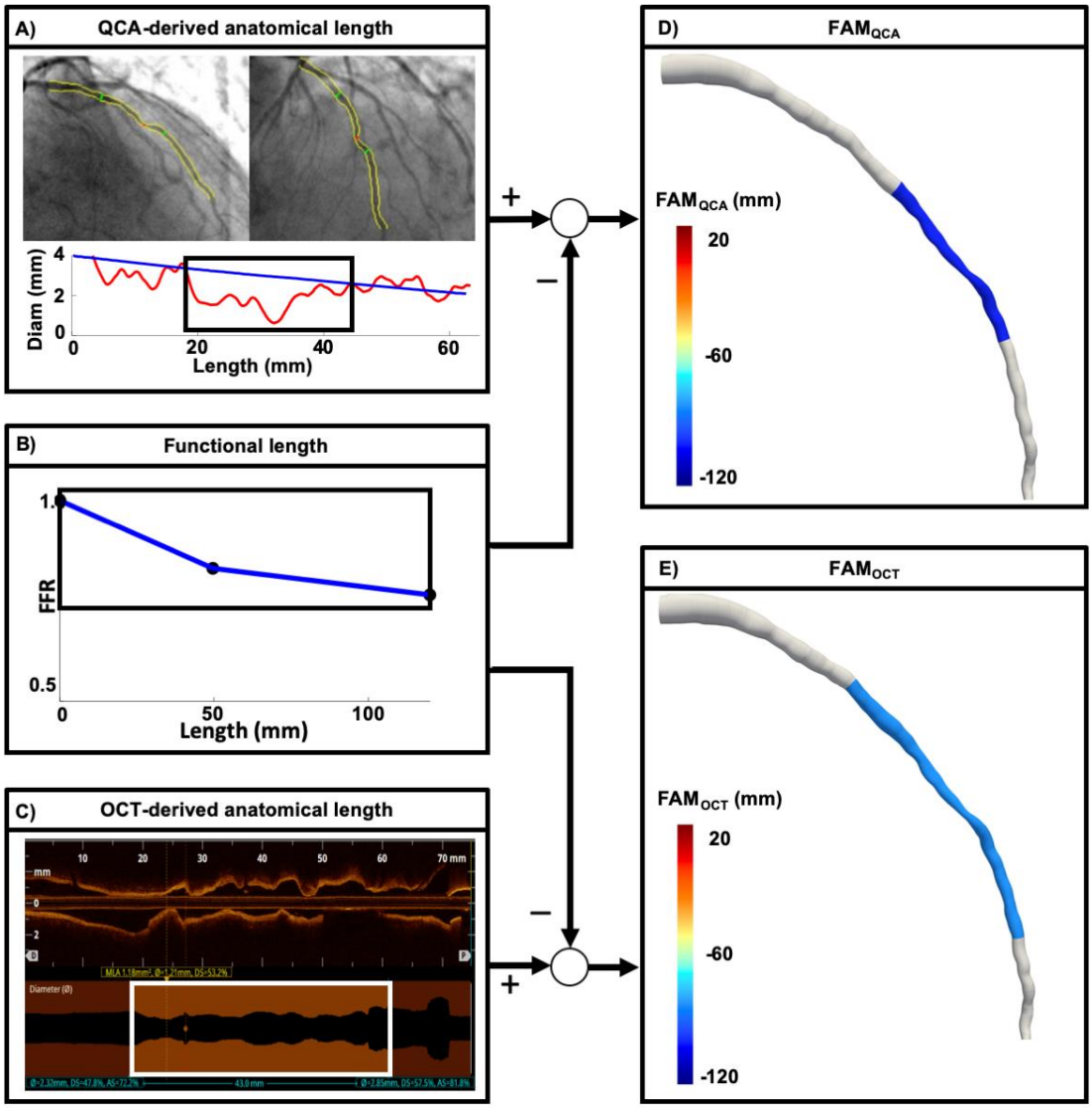

Figure 3. Definition of QCA-derived anatomical length, OCT-derived anatomical length, FAM_{QCA}, and FAM_{OCT}. An example of vessel with functional diffuse disease is considered. FAM_{QCA} is defined as the difference between QCA-derived anatomical length (panel A) and functional length (panel B) while FAM_{OCT} is defined as the difference between OCT-derived anatomical length (panel C) and functional length (panel B). The anatomical lesion derived from QCA or OCT is represented on the 3D geometric vessel reconstruction and color-coded using FAM_{QCA} or FAM_{OCT} (panels D and E, respectively). In both cases, functional lesion length is longer than anatomical lesion length (i.e. negative FAM).

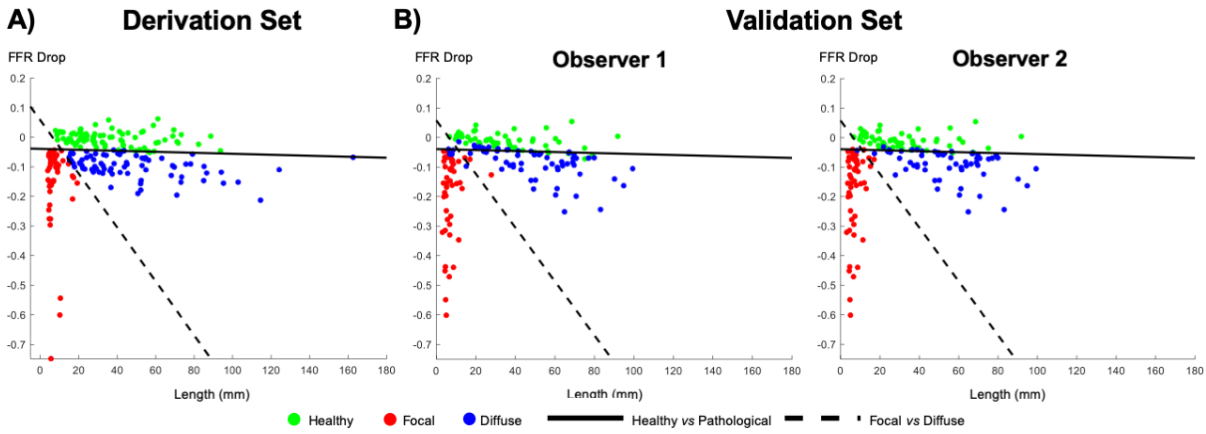

Figure 4. Development and performance of the automatic classifier. Healthy, focal disease and diffuse disease segments (green, red and blue, respectively) in length vs. FFR drop plane. The visual adjudication by two independent observers (CaC and SN) in the derivation set was used to develop the automatic classifier able to discriminate among healthy, focal disease and diffuse disease segments (panel A). The automatic classifier was then applied to the validation set (panel B). The performance of the classifier was evaluated by comparing with the visual adjudication by the two independent observers.

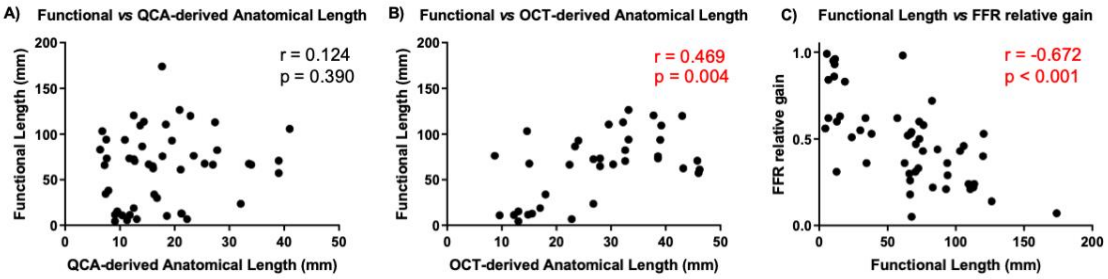

Figure 5. Scatter plots illustrating the correlations among functional length and QCA-derived anatomical length, OCT-derived anatomical length and FFR relative gain. The QCA-derived anatomical length was not correlated with functional length (panel A). The OCT-derived anatomical length was correlated with the functional length (panel B). The functional disease length was inversely correlated with the FFR relative gain (panel C).

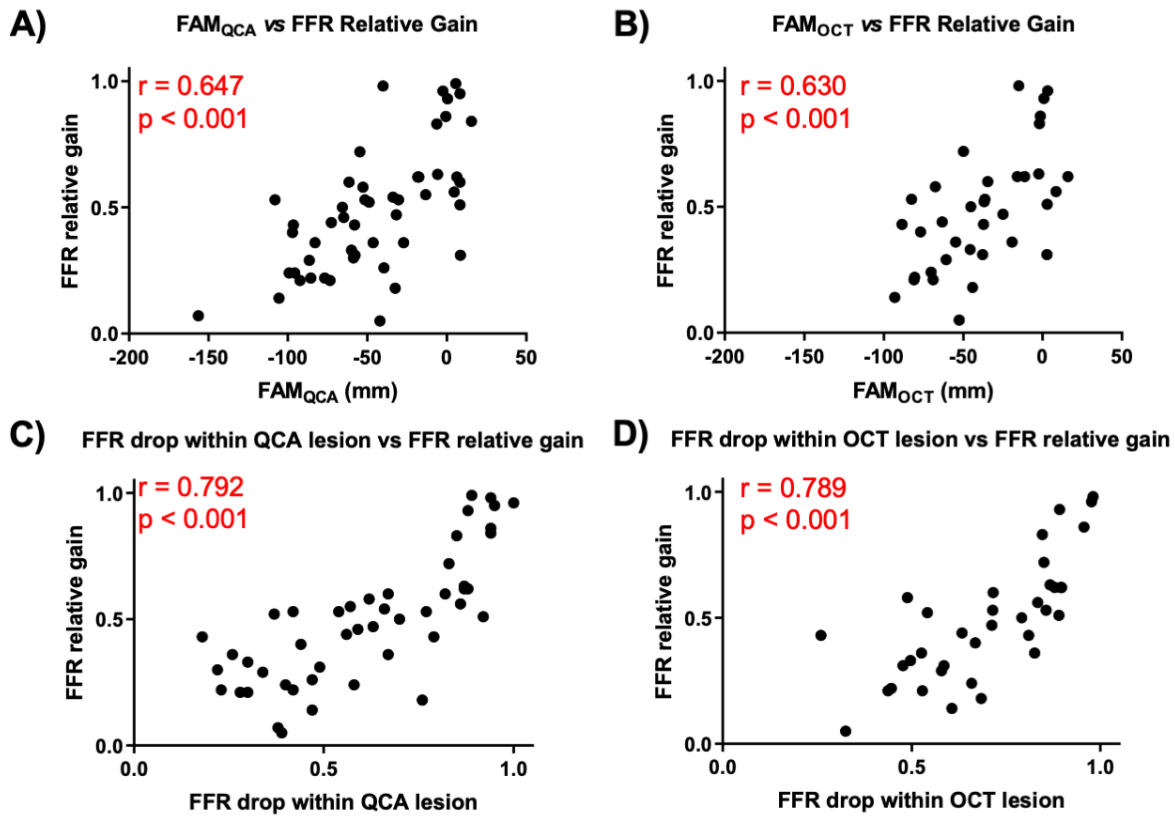

Figure 6. Scatter plots illustrating the correlations among FAM, FFR relative gain and among the FFR drop within the anatomical lesion and FFR relative gain. A direct significant association was found between the FAM_{QCA} and the FFR relative gain after PCI, i.e. the larger the FAM the higher the functional relative gain after PCI (panel A). A direct significant association was also found between the FAM_{OCT} and the FFR relative gain after PCI (panel B). The FFR drop within the QCA-derived anatomical lesion was strongly correlated with the functional relative gain after PCI, i.e. the larger the drop is attributable to the anatomical lesion with respect to the functional lesion, the better the PCI outcome (panel C). The FFR drop within the OCT-derived anatomical lesion was strongly correlated with the functional relative gain after PCI (panel D).

Supplementary Materials

Mismatch between the anatomical and functional extent of coronary artery disease

Maurizio Lodi Rizzini MSc; Jeroen Sonck MD; Diego Gallo PhD; Sakura Naguno MD, PhD; Takuya Mizukami MD, PhD; Fabrizio D'Ascenzo MD, PhD; Dimitri Buytaert MSc; Umberto Morbiducci PhD; Bernard de Bruyne MD, PhD, Claudio Chiastra, PhD and Carlos Collet MD, PhD

Address for Correspondence:
Carlos Collet MD, PhD
Cardiovascular Center Aalst, OLV Hospital,
Moorselbaan 164, Aalst, Belgium 9300
Telephone +3253724433
Fax: +32470795867
E-mail: carloscollet@gmail.com
Twitter @ColletCarlos

Supplementary Methods

Change points detection on FFR pullback curves

The detection of main changes in the distributional properties of FFR pullback curves was here addressed implementing a change points identification strategy. The implemented approach leads to a piece-wise linearization of FFR pullback curves based on a change points detection problem, where a change point is defined as a sample of the acquired FFR pullback curve at which an attribute of the curve suddenly changes.

Technically, a parametric global method already proposed elsewhere [1] was implemented here in MATLAB environment (MathWorks, Natick, MA, US) for FFR pullback change points identification. The steps of the implemented algorithm leading to a single change point detection are the following:

1. the FFR pullback curve is divided into two segments;
2. on each segment, the empirical estimation of the statistical property of interest is computed;
3. on each point of each segment the deviation from the empirical estimation is computed;
4. the total residual error is obtained by summation of deviations of segments points;
5. the location of the change point is identified iteratively minimizing the cost function represented by the total residual error.

The problem expressed by points 1-5 can be translated into an algorithm as explained in the followings. Given a generic FFR pullback curve, FFR = ($FFR_1, FFR_2, \ldots, FFR_N$), where FFR_i is the FFR value at i-th sample of the curve and N the total number of samples, the problem consists in finding the k-th sample minimizing the cost function

$$J(k) = \sum_{i=1}^{k-1} \Delta\left(FFR_i; \chi([FFR_1 \ldots FFR_{k-1}])\right) + \sum_{i=k}^{N} \Delta\left(FFR_i; \chi([FFR_k \ldots FFR_N])\right) \quad (1),$$

where χ is the empirical estimation of the statistical property of interest and Δ is the deviation measure. Since we are interested in highlighting changes in average value and slope along the FFR pullback curve, here a linear function was adopted as statistical property of interest. This is like to say that for a generic interval between points m and n along the FFR pullback curve (Figure S1), the terms at the right-hand side of Equation (1) can be expressed as:

$$\sum_{i=m}^{n} \Delta\left(FFR_i; \chi([FFR_m \ldots FFR_n])\right) = (n-m+1)\,\mathrm{var}([FFR_m \ldots FFR_n]) - \frac{\left(\sum_{i=m}^{n}\left(FFR_i; \mu([FFR_m \ldots FFR_n])\right)\left(i - \mu([FFR_m\ FFR_{m+1} \ldots FFR_n])\right)\right)^2}{(n-m+1)\,\mathrm{var}([FFR_m\ FFR_{m+1} \ldots FFR_n])} \quad (2)$$

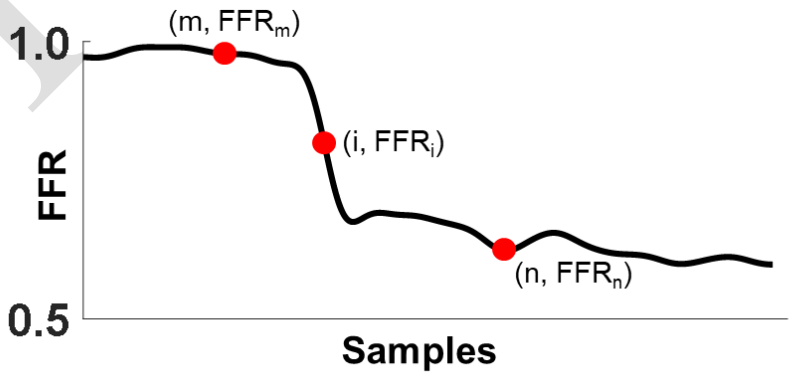

Figure S1. Explanatory case of FFR pullback curve with the generic points (m, FFR_m), (i, FFR_i) and (n, FFR_n).

A generic FFR pullback curve might have several change points, the number of change points being unknown a priori. Since adding change points decreases the residual error, the overfitting of the FFR curve is avoided by adding a penalty term which is a linear function of the number of change points to the cost function, which can be expressed as [2]

$$J(C) = \sum_{r=0}^{C} \sum_{i=k_r}^{k_{r+1}-1} \Delta\left(x_i; \chi\left(\left[FFR_{k_r} \dots FFR_{k_{r+1}-1}\right]\right)\right) + \beta C \qquad (3),$$

where k_r and k_C are the first and the last sample of the FFR pullback curve, respectively, C is the number of change points, and β is the fixed penalty term (set equal to 0.1 in this study). The minimization of the cost function was obtained implementing an algorithm based on dynamic programming with early abandonment [1].

Once the piece-wise linearization of FFR pullback curve has been carried out, each linearized segment of the curve was then characterized by two quantities (Figure S2): (1) the FFR drop, defined as the difference between the FFR values at the distal and at the proximal point of the segment; (2) the segment length, defined as the distance along the vessel axis between the distal point of the segment and the proximal point of the segment.

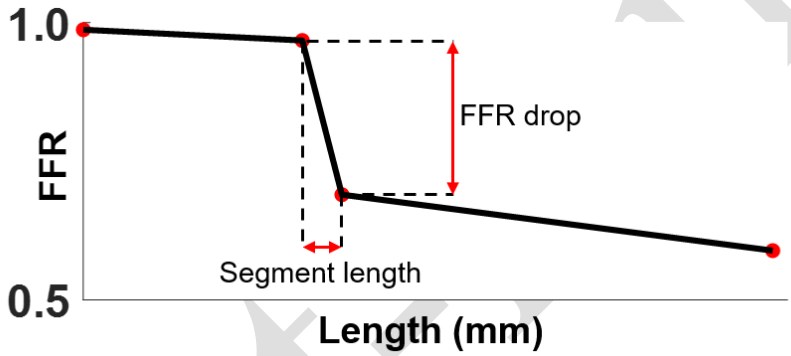

Figure S2. Explanatory case of piece-wise linearized FFR pullback curve with a graphical explanation of FFR drop and segment length.

On each segment a third quantity, the segment slope, was defined as the ratio between FFR drop and segment length.

Automatic segments classification

Two independent observers (CaC, SN) adjudicated by visual inspection each segment of the piece-wise linearized of FFR pullback curve as belonging to one of five segment phenotypes: (1) healthy segment; (2) focal disease segment; (3) diffuse disease segment; (4) pressure recovery segment; (5) artifact.

The automatic adjudication of each segment of the piece-wise linearized of FFR pullback curves to one of the defined five segment phenotypes was based on the application of a logistic regression model on FFR pullback curves segments from the derivation cohort (81 Patients). Technically, the logistic regression model was built on segments that obtained the same adjudication from the two observers (216 segments), while segments manually classified as artefacts were not considered. Two independent variables were considered in the logistic regression model to discriminate the segments: FFR drop and segment length.

Since the logistic regression provides a binary separation, a two-steps approach was implemented for the piece-wise linearized FFR pullback curve segments automatic adjudication:

step 1: separation between healthy and all (grouping focal and diffuse) diseased segments.

step 2: separation between focal and diffuse diseased segments.

In the healthy segment phenotype, pressure recovery segments were identified as the ones meeting all the following criteria: they have a positive FFR drop, they are contiguous to a diseased segment, and they are shorter than 20 mm.
The performance of the automatic adjudication was evaluated by comparison with the manual adjudication by the two observers (CaC; SN) on piece-wise linearized FFR pullback curves belonging to the validation cohort (50 patients, 179 segments). The results of the automatic adjudication are reported in Figure S3 in terms of accuracy, sensitivity, specificity.

Supplementary Results

Automatic classifier performances

The ability of the proposed automatic adjudication method in discriminating healthy, focal, and diffuse disease segments clearly emerges (Figure S3, panel A). Concerning the adjudication of healthy *vs.* pathological segments (Figure S3, panel B), the automatic adjudication provided an excellent performance in terms of accuracy (87.7% for CaC, 94.6% for SN) sensitivity (87.2% for CaC, 92.8% for SN) and specificity (88.7% for CaC, 98.2% for SN respectively). Concerning the adjudication of focal *vs.* diffuse disease (Figure S3, panel C), the automatic adjudication performance was also outstanding in terms of accuracy (94.6% for CaC, 96.4% for SN), sensitivity (91.9% for CaC, 98.3% for SN) and specificity (93.6% for CaC, 94.3% for SN).

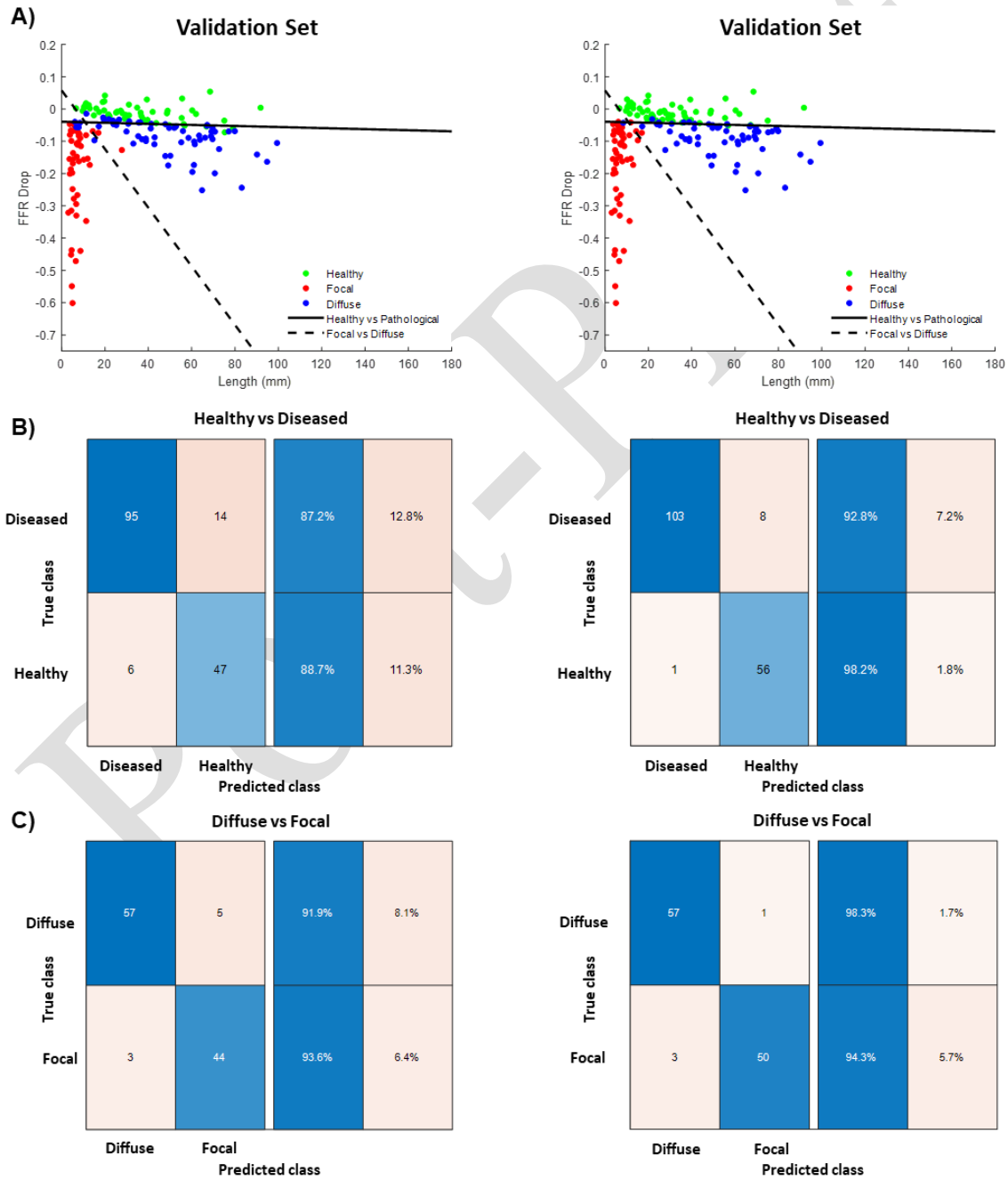

Figure S3. Results on the left are relative to observer CaC, on the right to observer SN. Panel A: Healthy, focal disease and diffuse disease segments (respectively, green, red, and blue) in length vs. FFR drop plane for the validation set. Panel B:

confusion matrices of the classification healthy *vs* pathological segments. Panel C: confusion matrices of the classification focal *vs* diffuse disease segments.

FAM sensitivity in serial lesions

Sensitivity of FAM_{QCA} and FAM_{OCT} to serial lesions was tested with two approaches: (1) considering only the contiguous segments in the definition of the functional length and (2) excluding serial lesions from the analysis. When considering only the contiguous segments to define the functional length, both FAM_{QCA} and FAM_{OCT} were still correlated with FFR relative gain after PCI (r=0.606, 95% CI 0.387 to 0.760, p<0.001, **Figure S4A** and r=0.560, 95% CI 0.326 to 0.729, p<0.001, **Figure S4C**). Excluding serial lesions (10 cases excluded for QCA and 8 cases excluded for OCT), both FAM_{QCA} and FAM_{OCT} were still correlated with FFR relative gain after PCI (r=0.708, 95% CI 0.502 to 0.838, p<0.001, **Figure S4B** and r=0.679, 95% CI 0.400 to 0.8427, p<0.001, **Figure S4D**).

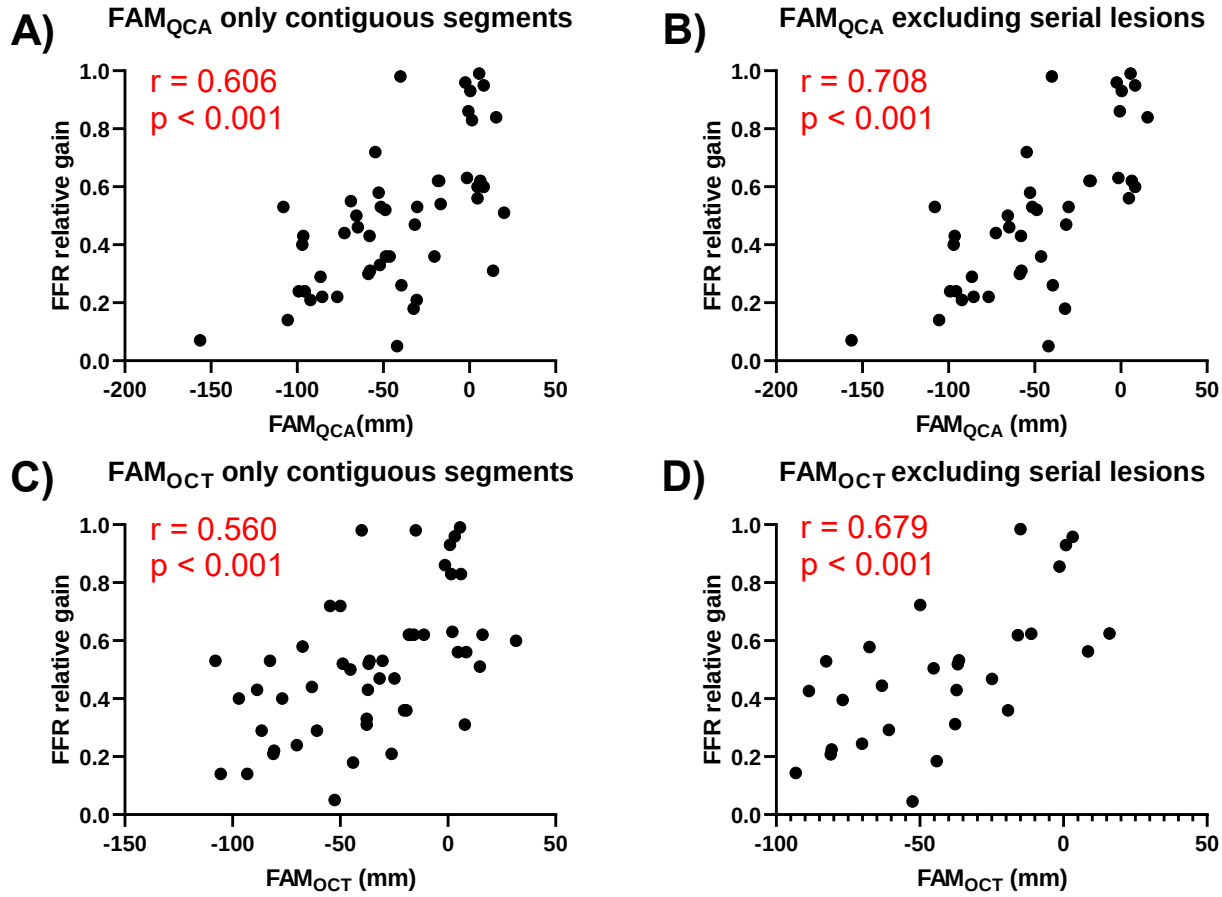

Figure S4. Sensitivity analysis to serial lesions of FAM_{QCA} and FAM_{OCT}. considering only the contiguous segments for the definition of the functional length, a direct significant association was found between FAM_{QCA} and FFR relative gain after PCI (panel A), and between FAM_{QCA} and FFR relative gain after PCI (panel C). Excluding serial lesions from analysis, a direct significant association was found between FAM_{QCA} and FFR relative gain after PCI (panel B), and between FAM_{QCA} and FFR relative gain after PCI (panel D).

Supplemental References

[1]. Killick, R., Fearnhead, P., Eckley, I.A., 2012. Optimal Detection of Changepoints With a Linear Computational Cost. J. Am. Stat. Assoc. 107, 1590–1598. https://doi.org/10.1080/01621459.2012.737745

[2]. Lavielle, M., 2005. Using penalized contrasts for the change-point problem. Signal Processing 85, 1501–1510. https://doi.org/10.1016/j.sigpro.2005.01.012